Electronic Supplementary Information

Engineering of Decameric D-fructose-6-phosphate Aldolase A by Combinatorial Modulation of Inter- and Intra-subunit Interactions

Xiaohong Yang,[ab†] Lian Wu, [cd†] Aipeng Li,[a] Lidan Ye, [*ab] Jiahai Zhou[*c] and Hongwei Yu[*ab]

[a]Key Laboratory of Biomass Chemical Engineering (Education Ministry), College of Chemical and Biological Engineering, Zhejiang University, Hangzhou 310027, China. E-mail: yuhongwei@zju.edu.cn, yelidan@zju.edu.cn

[b]Institute of Bioengineering, College of Chemical and Biological Engineering, Zhejiang University, Hangzhou 310027, China.

[c]State Key Laboratory of Bioorganic and Natural Products Chemistry, Center for Excellence in Molecular Synthesis, Shanghai Institute of Organic Chemistry, University of Chinese Academy of Sciences, 345 Lingling Road, Shanghai 200032, China. E-mail: jiahai@sioc.ac.cn

[d]The Key Laboratory of Synthetic Biology, and CAS Center for Excellence in Molecular Plant Sciences, Institute of Plant Physiology and Ecology, Chinese Academy of Sciences, Shanghai 200032, China.

† These authors contributed equally.

Table of Contents

Experimental Procedures

Materials

Taq DNA polymerase, restriction endonucleases, T4 DNA ligase and PrimerSTAR™ HS DNA polymerase were purchased from TAKARA Ltd. (Dalian, China). Protein marker was purchased from Sangon Biotech Ltd. (Shanghai, China). 2-thiophenecarboxaldehyde (**1a**), 3-thiophenecarboxaldehyde (**1b**) and 2-furaldehyde (**1d**) were purchased from Adamas-beta Ltd. (Shanghai, China). Benzothiophene-2-carboxaldehyde (**1c**), 2-pyridinecarboxaldehyde (**1e**) and hydroxyacetone (HA, **2**) were purchased from *Alfa Aesar* Ltd. (Shanghai, China). Other chemicals were purchased from Sangon Biotech Ltd. (Shanghai, China).

Mutagenesis

Recombinant plasmid pET-30a-*fsa*A (Gene Bank Accesion number BAA13552.1) was utilized as the template to introduce PCR-based site-directed mutagenesis following the QuikChange™ method (Stratagene, La Jolla, CA) according to the manufacturer's instructions. The double-site mutants were obtained using pET-30a-*fsa*A Q59T as template, and the triple-site mutants were obtained using pET-30a-*fsa*A I31T/Q59T as template. The recombinant plasmids were then transformed into chemically competent *E. coli* BL21 (DE3) following standard protocols. After sequencing verification, the recombinant plasmids were extracted and transformed into chemically competent *E. coli* BL21-pGro7 (DE3) containing pGro7 that harbors groEL-groES, which is a class of common molecular chaperones that can help proteins to fold correctly and is induced by L-arabinose.[1] To avoid the potential instability of mutants during heat treatment,[2] a His_6-tagged FSAA construct was used in mutagenesis, which meanwhile facilitated the purification of FSAA mutants by HisTrap affinity chromatography.

Cell Cultivation, Protein Expression and Purification

Cells were grown with shaking at 37 °C in 100 ml Luria–Bertani (LB) media containing 50 μg ml^{-1} of kanamycin and 20 μg ml^{-1} of chloramphenicol to an optical density of 0.6 at 600 nm. To induce protein expression, isopropyl-β-thiogalactopyranoside (IPTG, final concentration 100 μM) and L-arabinose (final concentration 1 mg mL^{-1}) were added and the temperature was lowered to 26 °C. After additional incubation of 8 h, the cultures were collected by centrifugation at 4000 × g, 4 °C and washed twice with phosphate buffer (50 mM, pH 7.4). The cell pellet was resuspended in phosphate buffer (50 mM, pH 8.0), and then lysed by sonication. Cellular debris was removed by centrifugation at 12,000 × g and 4 °C for 15 min. The enzyme was purified from the clear supernatant by HisTrap affinity column (GE Healthcare) following the manufacturer's instructions. Eluted fractions containing pure protein were pooled and loaded onto HiTrapTM desalting columns to remove imidazole and then redissolved in citric acid-sodium citrate buffer (0.1 M, pH 6.5). Protein concentrations were determined by the Bradford method and the expression of the wild-type FSAA as well as the mutants was examined by SDS-polyacrylamide gel electrophoresis (SDS-PAGE).

Activity Assay

To avoid spontaneous reaction, reactions were conducted in citric acid-sodium citrate buffer (0.1 M, pH 6.5) at 30 °C.[3] The initial reaction rate and maximum conversion rate of mutants were calculated using **1a**-**1e** as acceptor substrates. Reactions (total volume 300 μL) were conducted in 1.5-mL Eppendorf tubes, stirred with a vortex mixer (MS-100,

AOSHENG) at 1000 rpm and 30 °C. Concentrations of acceptors **1** and HA were 100 mM and 500 mM, respectively. The reactions were started by adding purified enzymes and the amount of enzymes and reaction time were adjusted to control the conversion below 5% in order to calculate the initial reaction rate (v_0, nmol min^{-1} mg^{-1} protein). Afterwards, the reactions were stopped by adding 900 µL methanol. The reaction mixtures were then incubated in an ice bath for 3 h, followed by high performance liquid chromatography (HPLC) analysis. Conversion rates were calculated after agitating for 24 h. The reaction mixtures were then extracted using ethyl acetate, dried and redissolved in isopropanol for diastereomeric ratio (dr) and enantiomeric excess (ee) analysis.

Determination of Apparent Kinetic Parameters for HA and 2-thiophenecarboxaldehyde (1a)

The apparent kinetic parameters including Michaelis constant (K_{m}^{app}) and turnover number (K_{cat}^{app}) for the nucleophile HA and acceptor **1a** catalyzed by wild-type FSAA, I31T FSAA, Q59T FSAA, I195Q FSAA and the triple-site variant I31T/Q59T/I195Q FSAA were determined via Lineweaver-Burk double reciprocal plots. Analytical scale reactions (total volume 300 µL) were conducted at 30 °C in Eppendorf tubes (1.5 mL), stirred using a vortex mixer (MS-100, AOSHENG) at 1000 rpm.

*Kinetic parameters for 2-thiophenecarboxaldehyde **1a**.* HA (200 mM) was dissolved in citric acid-sodium citrate buffer (0.1 M, pH 6.5). Different concentrations of **1a** were added into the reaction mixture (10, 20, 45, 60, 80, 100, 150 and 200 mM for wild-type FSAA; 5, 10, 20, 30, 45, 60, 80, 100 and 200 mM for I31T FSAA; 5, 10, 20, 30, 45, 60, 100, 150 and 200 mM for Q59T FSAA; 5, 20, 30, 45, 60, 80, 100 and 150 mM for I195Q FSAA; 5, 10, 30, 45, 60, 80, 100, 150 and 200 mM for I31T/Q59T/I195Q FSAA). To this mixture, the wild-type FSAA, I31T FSAA, Q59T FSAA, I195Q FSAA and I31T/Q59T/I195Q FSAA (containing 0.15 to 0.36 mg of protein) were added to start the reaction (total final volume 300 µL). Conversion was controlled below 5%. Reaction was stopped by adding 900 µL methanol at different time (in a range between 30-45 min), centrifuged, and then analyzed by HPLC.

Kinetic parameters for HA. **1a** (100 mM) was dissolved in citric acid-sodium citrate buffer (0.1 M, pH 6.5). Different concentrations of HA were added into the reaction mixture (10, 20, 40, 60, 80, 100, 200 and 300 mM for wild-type FSAA; 10, 20, 40, 60, 100, 150, 200 and 300 mM for I31T FSAA; 10, 20, 40, 60, 80, 100, 150, 200 and 300 mM for Q59T FSAA; 10, 20, 40, 60, 100, 150, 200 and 300 mM for I195Q FSAA; 10, 20, 60, 100, 150, 200 and 300 mM for I31T/Q59T/I195Q FSAA). To this mixture, wild-type FSAA, I31T FSAA, Q59T FSAA, I195Q FSAA and I31T/Q59T/I195Q FSAA (containing 0.15 to 0.36 mg of protein) were added to start the reaction (total final volume 300 µL). Conversion was controlled below 5%. Reaction was stopped by adding 900 µL methanol at different time (in a range between 30-60 min), centrifuged, and then analyzed by HPLC.

X-ray Structure Determination

The variant I31TQ59TI195Q FSAA (PDB ID: 5ZOL) was crystallized in 2 M NaCl, 16% PEG 6000, 3% D-(+)-trehalose dihydrate at 18 °C using the sitting-drop vapor diffusion method. Proteins (at 10 mg/mL, in 25mM Tris-HCl pH 7.5, 150 mM NaCl) were mixed in a 1:1 ratio with the reservoir solution in a final volume of 2 µL and equilibrated against the reservoir solution. The complex crystals of variant with HA and **1a** were prepared by soaking the crystals of variant in reservoir containing 100 mM HA and 50 mM **1a** for 3-5 min, and **1a** was phase splitting with reservoir. All crystals were flash cooled in liquid nitrogen after being dipped into paratone oil. Diffraction data of mutant complex were collected

at the wavelength of 0.97853 Å on SSRF beamline 19U1 of the National Center for Protein Science in Shanghai (China). Since the unit cell was huge containing ten molecules, we cut the resolution using the distance of 400 nm to collect the data, avoiding overlapping of dots. All data collection was performed at 100 K. All data sets were indexed, integrated, and scaled using the HKL3000 package.[4] The complex structure of variant with the donor HA and acceptor **1a** was solved by molecular replacement method using the program PHASER[5] and the structure of wild-type FSAA (PDB ID: 1L6W) was used as a search model. Rounds of automated refinement were performed with PHENIX[6] and the models were extended and rebuilt manually with COOT.[7] The structure of the I31T/Q59T/I1954Q-HA-**1a** complex has been refined to 2.17 Å. The statistics for data collection and crystallographic refinement are summarized in Table S2.

Computational Methods

The coordinates of decameric wild-type *E. coli* FSAA were obtained from the Protein Data Bank (PDB ID: 1L6W).[8] To build the minimal functional unit for calculation as well as to simulate the interface interactions between adjacent subunits, a large fragment from chain A with residues 1-199[9] and the entire chain B were employed. The resolved crystal structure of I31T/Q59T/I195Q FSAA (PDB ID: 5ZOL) was exploited to build a functional unit for the mutant in the same way. Based on proposed mechanism,[10] HA was covalently bound to acceptor **1a** to generate a hemiaminal intermediate. This intermediate was then covalently bound to Lys85 to provide a productive binding model for simulation. Nonpolar hydrogen atoms were added to the enzyme structure using the AMBER 14 simulation package.[11] Other parameters were set according to the previous study.[3] During simulation, 2500 cycles of steepest descent followed by 2500 cycles of conjugate gradient minimization were first applied to remove potential collision contacts with the added water molecules. After gradually heating to 303 K over the course of 50 ps, the system was then set with a 50 ps of density equilibration at a constant temperature of 303 K. Only water molecules could move freely, and the rest parts of the system were restrained during these two steps described above. After density equilibration, the whole system could move freely. Then the system was equilibrated through conducting a 1 ns constant-pressure and constant-temperature (NPT) ensemble simulation. Finally, another 6 ns (corresponding to 1500 trajectory frames, Fig. S6) production run in the NPT ensemble was performed at 303 K. Langevin thermostat was applied to maintain the temperature of the system. The nonbonding cutoff distance was set to 8.0 Å and simulation snapshots were saved every 2 ps for analysis. The conformation of each simulation was analyzed using the cpptraj program in the AMBER 14 package and VMD.[12] The calculation and decomposition of binding free energy, ΔG_{bind}, between the ligand and the enzyme were conducted using MM/PBSA method in AMBER 14. MM/PBSA computes the binding free energy by using a thermodynamic cycle that combines the molecular mechanical energies with the continuum solvent approach. The binding free energy ΔG_{bind} between a ligand and a receptor to form a complex was calculated as follows:

$$\Delta G_{binding} = \Delta H - T\Delta S \approx \Delta E_{MM} + \Delta G_{sol} - T\Delta S$$

$$\Delta E_{MM} = \Delta E_{internal} + \Delta E_{electrostatic} + \Delta E_{vdw}$$

$$\Delta E_{sol} = \Delta E_{PB} + \Delta E_{np}$$

where ΔE_{MM}, ΔG_{sol} and $T\Delta S$ stand for the changes of the gas-phase MM energy, the solvation free energy and the conformational entropy, respectively. ΔE_{MM} is the sum of $\Delta E_{internal}$ (bonds, angles, and dihedrals energy), $\Delta E_{electrostatic}$ (electrostatic energy), and ΔE_{vdw} (van der Waals). G_{sol} accounts for the solvation energy which can be divided into the electrostatic solvation energy (polar part), ΔG_{PB} and the nonelectrostatic solvation energy (nonpolar part), ΔG_{np}. In this

study, "the same trajectory method" was used in all analyses, so the internal energy term ($\Delta E_{internal}$) was zero. A total of 200 conformations (corresponding to 200 trajectory frames) were extracted from the stable part of trajectory after 2.5 ns and used for MM/PBSA analysis. The volume of binding pocket was calculated by POVME 2.0 software.[13] Figures were prepared by UCSF Chimera package[14] and PyMOL.[15]

Whole-cell Catalyzed Aldol Addition of HA (2) to Heteroaromatic Aldehydes (1)

Recombinant *E. coli* overexpressing wild-type FSAA and variant I31T/Q59T/I195Q FSAA were used respectively as whole-cell catalysts. Reactions (total volume as 300 µL) were conducted at 30 °C in citric acid-sodium citrate buffer (0.1 M, pH 6.5) with agitation (220 rpm). Concentrations of acceptor substrates **1a**, **1b**, **1c**, **1d** and **1e** were 400 mM, 350 mM, 300 mM, 500 mM and 500 mM, respectively. Concentrations of donor **2** were 5 times as high as those of the corresponding acceptor substrates. The catalyst loading was 80 g/L (wet cell weight) of resting cells. Reaction was stopped by adding 900 µL methanol at different time, centrifuged, and then analyzed by HPLC.

Synthesis of Products 3a-3e Using Whole-cell Catalyst and Chemical Catalyst

Synthesis using whole-cell catalyst

The reactions (20 mL total volume) containing acceptors (300 mM) and hydroxyacetone (1.5 M) were conducted in 100 mL capped conical-bottom flasks, and then incubated with recombinant whole cells overexpressing the variant I31T/Q59T/I195Q FSAA (60 g/L, wet cell weight) in citric acid-sodium citrate buffer (0.1 M, pH 6.5) at 30 °C with agitation (220 rpm) for 48 h.

Then the mixture of **1a** was extracted with a 1:2 mixture of ethyl acetate-hexane. The organic layer was discarded to remove residual substrates. The aqueous phase was extracted again with dichloromethane, and the organic layer was concentrated under vacuum yielding the corresponding product **3a** (18% isolated yield) without further purification. The mixture of **1b** as well as **1c** was extracted with hexane. After removal of the organic layer, the aqueous phase was extracted again with dichloromethane, and the organic layer was concentrated under vacuum. After washing with water, the product **3b** (34.8% isolated yield) and **3c** (37% isolated yield) were lyophilized. The mixture of **1d** was extracted with a 1:4 mixture of ethyl acetate-hexane. After removal of the organic layer, the aqueous phase was extracted again with dichloromethane, and the organic layer was concentrated under vacuum, yielding corresponding product **3d** (44% isolated yield) without further purification.

Synthesis using chemical catalyst

For **1a**-**1e**, a MeOH solution (10 ml total volume) containing acceptors (500 mM) and hydroxyacetone (500 mM) were stirred with 5% aqueous sodium hydroxide (0.34 ml) in a 50 mL capped conical-bottom flask at room temperature. After 30 min or more according to the results of thin-layer chromatography (TLC), excessive iced water containing 10% acetic acid was poured into the solution.

The racemic **3a** (22% isolated yield), **3b** (16% isolated yield), **3c** (60.5% isolated yield) and **3d** (38% isolated yield) were purified as described above. To obtain racemic **3e** (28% isolated yield), the mixture of **1e** was extracted with a 3:1 mixture of ethyl acetate-hexane. The organic layer was discarded to remove residual substrates. The aqueous phase was extracted again with dichloromethane, and the organic layer was concentrated under vacuum.

Stereoselectivity Assay

The racemic products **3a**-**3e** derived from NaOH catalysis together with the corresponding chiral products synthesized by whole-cell catalyst were analyzed by ^{1}H NMR, followed by optical rotation measurement using a Rudolph Research Analytical Autopol IV Polarimeter (Fig. S8). The absolute configuration of enzymatically catalyzed diols **3a** and **3c** was assigned as (3*S*, 4*S*) by comparing the analysis data with reported values.[16] The absolute configuration of enzymatically catalyzed diols **3a** was also confirmed by the crystal structure. For enzymatically catalyzed products **3b**, **3d** and **3e**, the corresponding absolute configurations could not be assigned at present since related references are not available.

HPLC Analysis

For determination of enzyme activity, HPLC analysis was executed with a CHIRALPAK AD-RH column (5μm, 4.6×150 mm) at 254 nm. Samples (injection volume 20 μL) were eluted under the following conditions:

For **1a** and **1b**, the mobile phase was composed of acetonitrile and water (25/75, v/v) at a flow rate of 1 mL min^{-1}.

For **1c**, the mobile phase was composed of acetonitrile and water (50/50, v/v) at a flow rate of 1 mL min^{-1}.

For **1d**, the mobile phase was composed of acetonitrile and water (25/75, v/v) at a flow rate of 0.6 mL min^{-1}.

For **1e**, the mobile phase was composed of acetonitrile and water (20/80, v/v) at a flow rate of 0.6 mL min^{-1}.

The diastereomeric ratio (dr) and enantiomeric excess (ee) of the products **3a**, **3c**,**3d** and **3e** were analyzed via HPLC using an AD-H chiral column.

For **3a** (UV detector at 240 nm) and **3d** (UV detector at 230 nm), the mobile phase was composed of *n*-hexane and *iso*-propanol (93/7, v/v) at a flow rate of 1 mL min^{-1}.

For **3c** (UV detector at 254 nm) and **3e** (UV detector at 254 nm), the mobile phase was composed of *n*-hexane and *iso*-propanol (90/10, v/v) at a flow rate of 1 mL min^{-1}.

The dr values and ee values of the products **3b** were analyzed via HPLC using an AS-H chiral column and a UV detector at 240 nm. The mobile phase was composed of *n*-hexane and *iso*-propanol (90/10, v/v) at a flow rate of 1 mL min^{-1}.

High-performance Liquid Chromatography-tandem Mass Spectrometry

The high-performance liquid chromatography-tandem mass spectrometry (HPLC-MS/MS) was conducted to confirm the structure of **3b** as previsouly described.[3] HPLC was performed on U3000 (Thermo Fisher Scientific) equiped with a CHIRALPAK AD-RH column (5μm, 4.6×150 mm), and the signals were detected at 254 nm. The mobile phase was the same as described above in the **HPLC analysis** section.

Supplementary Tables

Table S1. PCR primers used for construction of the mutants.

Primers		Oligonucleotides[a]
I31T FSAA	Forward	CCACTAACCCAAGCACTATCGCCGCGGGTAAAAAACCGC
	Reverse	TTACCCGCGGCGATAGTGCTTGGGTTAGTGGTCACACCC
I31W FSAA	Forward	CCACTAACCCAAGCTGGATCGCCGCGGGTAAAAAACCGC
	Reverse	TTACCCGCGGCGATCCAGCTTGGGTTAGTGGTCACACCC
Q59T FSAA	Forward	GGCGTCTGTTTGCCACCGTAATGGCTACCACTGCCGAAG
	Reverse	GTGGTAGCCATTACGGTGGCAAACAGACGCCCCTGACCG
L163V FSAA	Forward	CGCAGGCGAAAGTGGTGGCAGCGAGTTTCAAAACCCCGC
	Reverse	TTGAAACTCGCTGCCACCACTTTCGCCTGCGGCGCATGC
I195S FSAA	Forward	TGGCACAACAGATGTCAAGCTATCCGGCGGTTGATGCCG
	Reverse	ACCGCCGGATAGCTTGACATCTGTTGTGCCACATCCAGT
I195Q FSAA	Forward	TGGCACAACAGATGCAGAGCTATCCGGCGGTTGATGCCG
	Reverse	ACCGCCGGATAGCTCTGCATCTGTTGTGCCACATCCAGT
S196E FSAA	Forward	CACAACAGATGATTGAATATCCGGCGGTTGATGCCGCTG
	Reverse	TCAACCGCCGGATATTCAATCATCTGTTGTGCCACATCC

[a] The mutated sites are underlined

Table S2. X-ray data collection and refinement statistics.

Name	I31T/Q59T/I195Q FSAA
PDB ID	5ZOL
Data collection	
Beamline	SSRF-BL19U1
Wavelength(Å)	0.97853
Space group	*P3221*
Unit cell parameters(Å)	a = 103.1
	b = 103.1
	c = 493.3
Resolution(Å)[a]	2.172
No of measured reflections	1429091
No of unique reflections	195445
Redundancy	7.3 (7.6)
Completeness (%)[a]	99.5 (99.5)
Average(I/σ)[a]	17.2 (1.3)
R_{merge} (%)[a], [b]	0.105 (1.4)
Refinement	
No of reflections(work/free)	184281 (9215)
R_{work}/R_{free}[c]	0.2002 / 0.2479
Number of non-H atoms	
Protein atoms	15767
Water	1051
Average B factor[A^2]	32.9
Bond lengths(Å)	0.009
Bond angles (°)	0.957
Ramachandran plot favored (%)	96.99
Ramachandran plot allowed (%)	2.83
Ramachandran plot outlier (%)	0.18

[a] Numbers in parentheses are values for the highest-resolution shell. [b] $R_{merge} = \Sigma_{hkl}\Sigma_i|I_i - \langle I\rangle|/\Sigma_{hkl}\Sigma_i|\langle I\rangle|$, where I_i is the intensity for the *i*th measurement of an equivalent reflection with indices h, k, and l. [c] R_{free} was calculated with the 5% of reflections set aside randomly throughout the refinement.

Table S3. Apparent K_{m}^{app} and K_{cat}^{app} values of the wild-type FSAA (WT) and variants towards acceptor **1a** and donor (HA, **2**).

FSAA catalysts	Substrate	K_{m}^{app} (mM)	K_{cat}^{app} (s^{-1})	$K_{\mathrm{cat}}^{app}/K_{m}^{app}$ (s^{-1} mM^{-1})
WT	**1a**	54 ± 1.84	47.7 ± 3.39	0.88 ± 0.09
I31T	**1a**	49 ± 2.12	168.7 ± 5.23	3.44 ± 0.04
Q59T	**1a**	101 ± 2.69	916.7 ± 1.84	9.08 ± 0.22
195Q	**1a**	88 ± 2.83	194.3 ± 3.82	2.21 ± 0.11
I31T/Q59T/I195Q	**1a**	62.6 ± 1.98	6461 ± 9.89	103 ± 3.11
WT	**2**	20 ± 0.56	47.7 ± 2.97	2.39 ± 0.08
I31T	**2**	152 ± 5.65	166.8 ± 3.25	1.10 ± 0.06
Q59T	**2**	46.5 ± 3.68	916.7 ± 5.09	19.71 ± 1.67
195Q	**2**	21 ± 1.41	183.3 ± 6.22	8.73 ± 0.29
I31T/Q59T/I195Q	**2**	77.6 ± 3.25	6340 ± 21.2	82 ± 3.15

Table S4. B-factor of the C-terminal α-helix consisting of residues 187-215 from the wild-type FSAA (WT) and I31T/Q59T/I195Q FSAA (MT).

Residue number	Average B-factor of ten chains [A^2]	
	WT	MT
187	13.06	28.73
188	15.29	40.39
189	15.91	49.33
190	12.40	35.61
191	13.54	43.34
192	24.80	63.27
193	17.57	52.26
194	16.41	56.32
195	16.96	68.84
196	16.52	67.77
197	13.85	55.89
198	14.86	46.72
199	12.86	41.07
200	13.74	38.42
201	17.68	46.46
202	15.02	41.35
203	14.82	40.18
204	17.40	42.79
205	18.61	46.31
206	22.57	50.31
207	16.60	46.00
208	24.17	64.67
209	26.18	61.03
210	22.04	53.53
211	22.24	50.93
212	31.31	71.46
213	29.34	61.83
214	29.39	59.35
215	28.46	58.11

Table S5. Hydrogen bond analysis of the wild-type FSAA (WT) and I31T/Q59T/I195Q FSAA (MT).

Residue pairs	Hydrogen bond	WT	MT
:28 - :31	Occupancy (%)	24.5	71.6
	Distance (Å)	2.9	2.71
	Angle (°)	158.3	163.2
:lig[a] - :28	Occupancy (%)	24.8	40.2
	Distance (Å)	2.89	2.73
	Angle (°)	154.2	155.8
:59 - :WAT[b]	Occupancy (%)	82.8	0
	Distance (Å)	2.75	--
	Angle (°)	160.9	--
:WAT - :131	Occupancy (%)	59.3	95.7
	Distance (Å)	2.74	2.72
	Angle (°)	151.2	161.2
:lig - :WAT	Occupancy (%)	10	54.2
	Distance (Å)	2.76	2.8
	Angle (°)	158.5	160
:195 (backbone) - :solvent	Occupancy (%)	9.8	27.3
	Distance (Å)	2.74	2.75
	Angle (°)	160.8	160.5
:195 (side chain) - :solvent	Occupancy (%)	0	20
	Distance (Å)	--	2.77
	Angle (°)	--	159.2

[a] Ligand in molecular dynamic simulations. [b] Catalytic water for proton transfer.

Table S6. Decomposition of binding free energy for individual residues in the wild-type FSAA (WT) and mutant I31T/Q59T/I195Q FSAA (MT).

Key residue number	Total energy (kcal mol^{-1})	
	WT	MT
28	-1.273	-2.011
31	-0.333	0.023
59	0.456	-0.156
85[a]	-1.399	-4.689
109	2.249	1.273
131	3.101	0.418
195	0.003	0.002

[a] The catalytic lysine.

Table S7. Binding free energies of the enzyme-substrate complexes for the wild-type FSAA (WT) and I31T/Q59T/I195Q FSAA (MT).

Enzyme	$\Delta G_{binding}$ (kcal mol^{-1}) [a]
WT	-17.56 ± 4.5
MT	-21.43 ± 2.9

[a] The binding free energy is calculated by the MM/PBSA program of AMBER software package.

Table S8. Calculation of distance between the Cα of residues involved in interface interactions of the wild-type FSAA (WT) and mutant I31T/Q59T/I195Q FSAA (MT).

Enzyme	Distance (Å)		
	:29@CA-:207@CA	:30@CA-:210@CA	:33@CA-:214@CA
WT	6.0	5.9	5.5
MT	7.8	7.2	5.4

Supplementary Figures

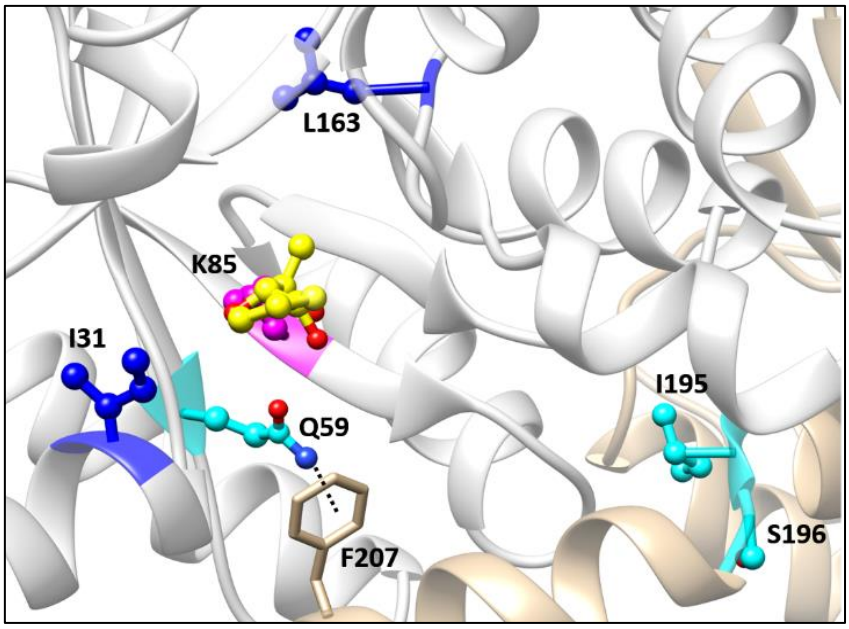

Fig. S1 A snapshot of the structure of the wild-type FSAA (WT) bound with the ligand derived from molecular dynamics (MD) simulation. The adjacent subunits of WT are shown in silver and golden, respectively. Ligand is shown in yellow and the active site Lys85 is shown in magenta. Residue 31 and residue 163 for modulation of intra-subunit interactions are shown in blue. Residue 59, residue 195 and residue 196 for modulation of inter-subunit interactions are shown in cyan. The putative NH/π interaction between residue 59 and residue 207 is shown as a dark dashed line.

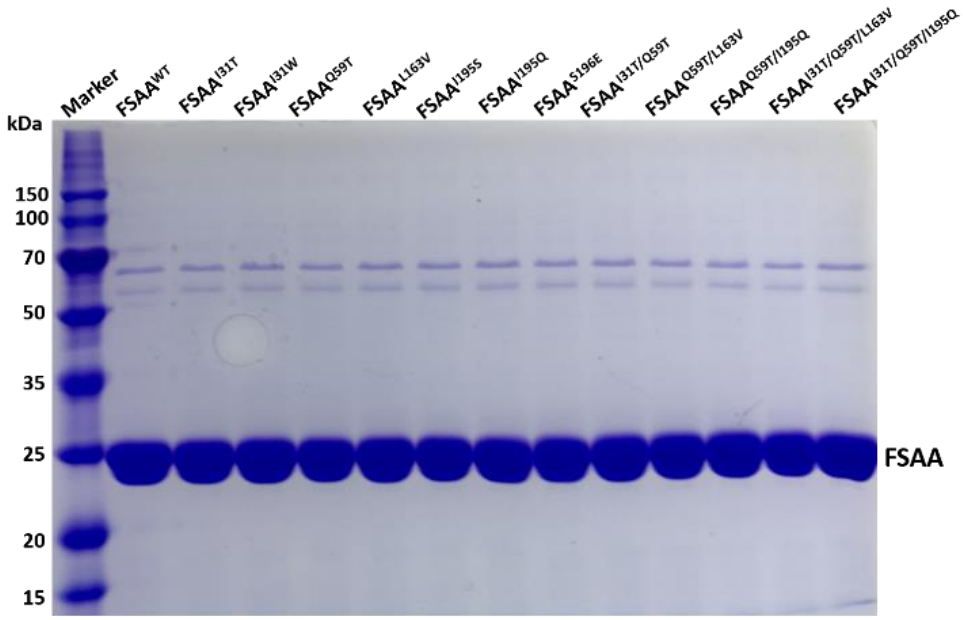

Fig. S2 SDS-PAGE analysis of purified wild-type FSAA (WT) and mutants.

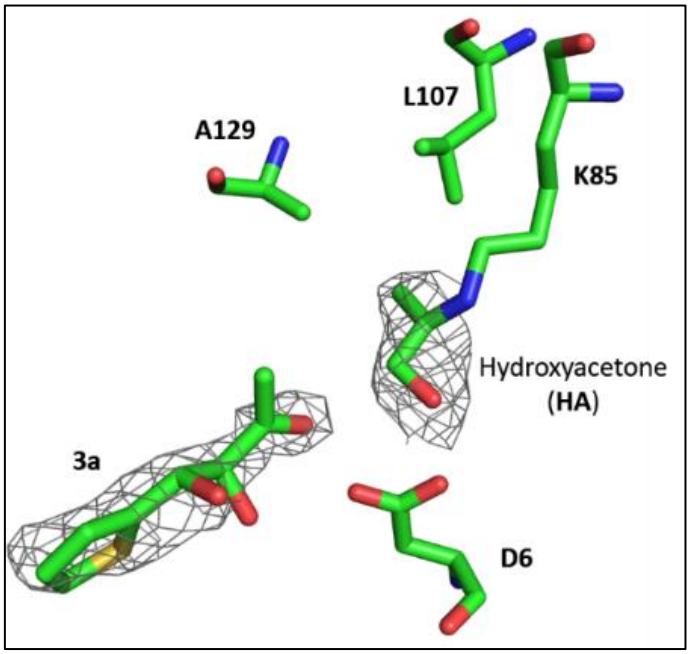

Fig. S3 Electron density map of donor hydroxyacetone (HA) covalently bound to the catalytic lysine residue (K85) and product **3a** in I31T/Q59T/I195Q FSAA at 2.17 Å resolution. The map is contoured at 1σ (grey).

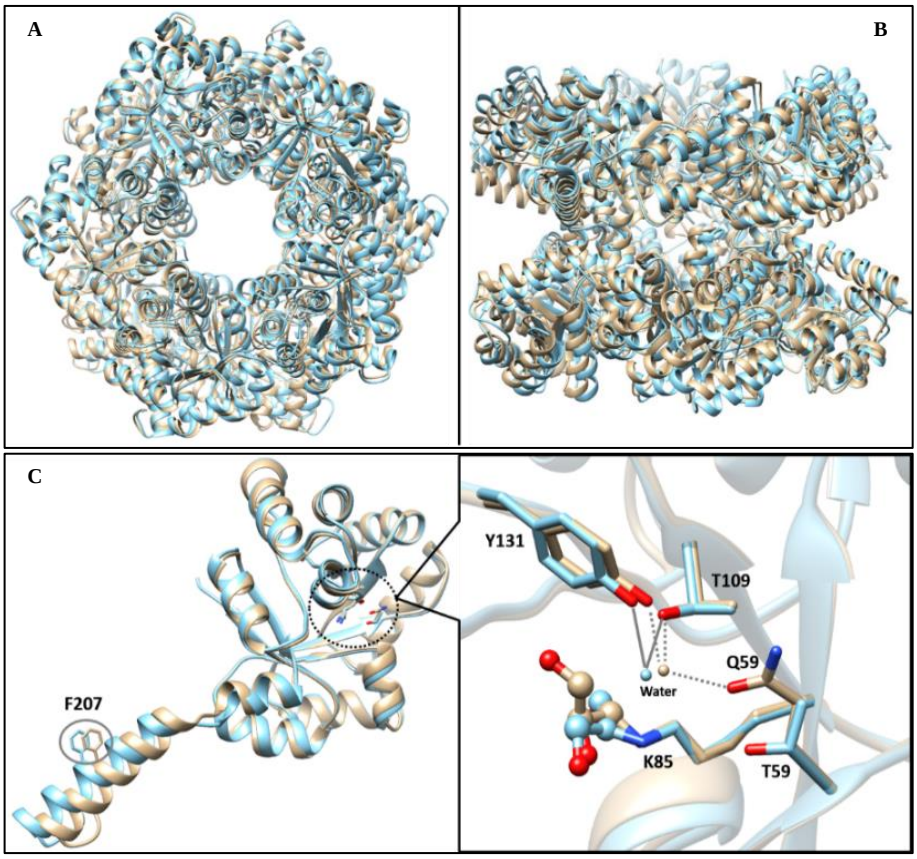

Fig. S4 Crystal structure alignment of wild-type FSAA (WT, gold) and I31T/Q59T/I195Q FSAA (cyan). Overall alignment in top view (**A**) and side view (**B**), and single subunit alignment (**C**). Hydrogen bonds between a catalytic water respectively with the active site residues Gln59, Thr109 and Tyr132 of the WT are shown as grey dashed lines, and hydrogen bonds between a catalytic water respectively with the active site residues Thr109 and Tyr132 of mutant I31T/Q59T/I195Q are shown as grey solid lines. The covalent ligands of the WT (oxidation of glycerol) and the mutant (hydroxyacetone) are both shown in ball-stick form, while active site residues are shown as sticks.

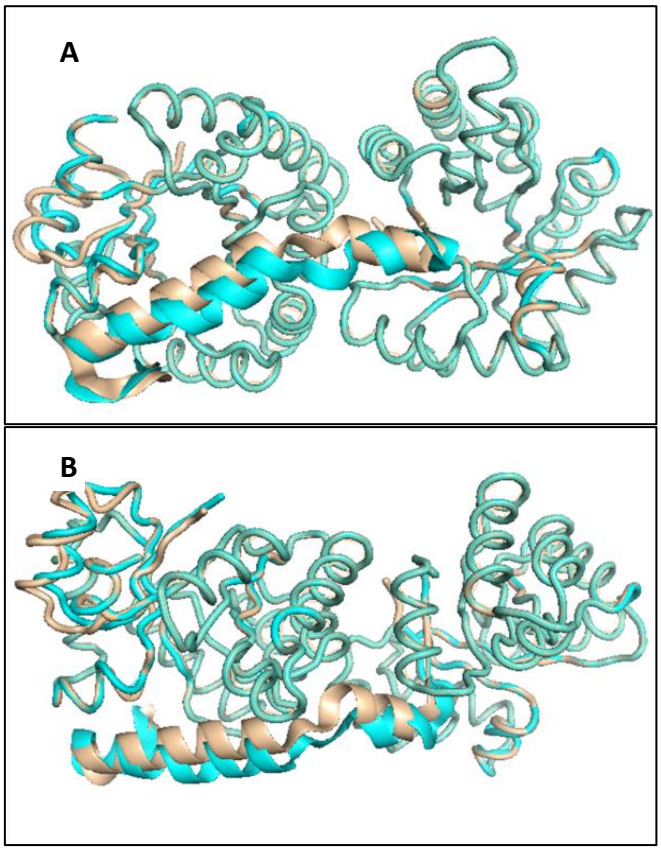

Fig. S5 Structural comparison of wild-type FSAA (WT) and I31T/Q59T/I195Q FSAA (MT) with structures derived from molecular dynamics (MD) simulations. Side view (**A**) and top view (**B**) of overall structure alignment for WT shown as wheat and MT shown as cyan. Target α-helix is shown as cartoon oval and others are shown as cartoon tubes

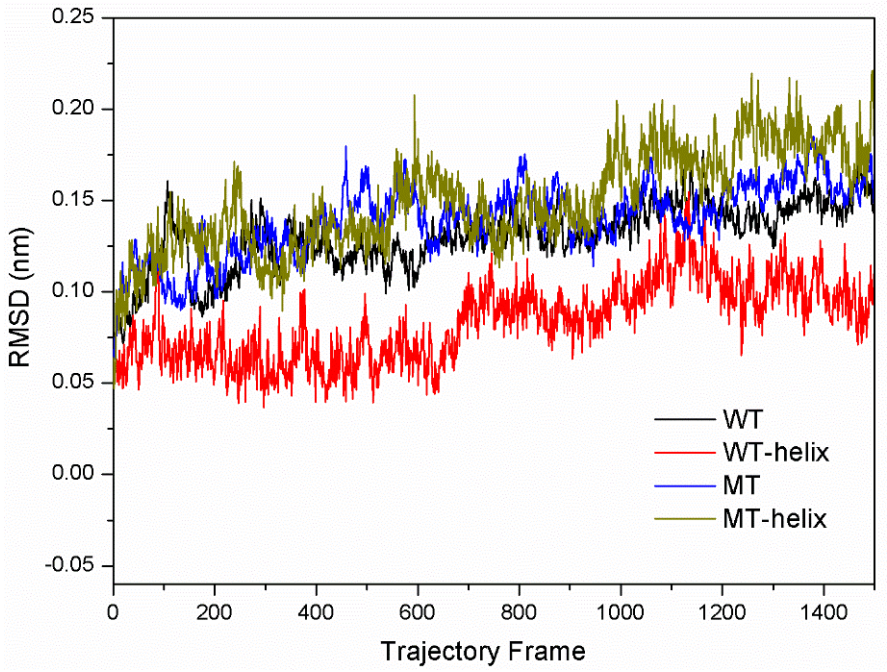

Fig. S6 Root-mean-square deviation (RMSD) during the molecular dynamics (MD) simulations. **WT** for backbone of wild-type FSAA; **WT-helix** for the C-terminal α-helix of wild-type FSAA; **MT** for backbone of I31T/Q59T/I195Q FSAA; **MT-helix** for the C-terminal α-helix of I31T/Q59T/I195Q FSAA.

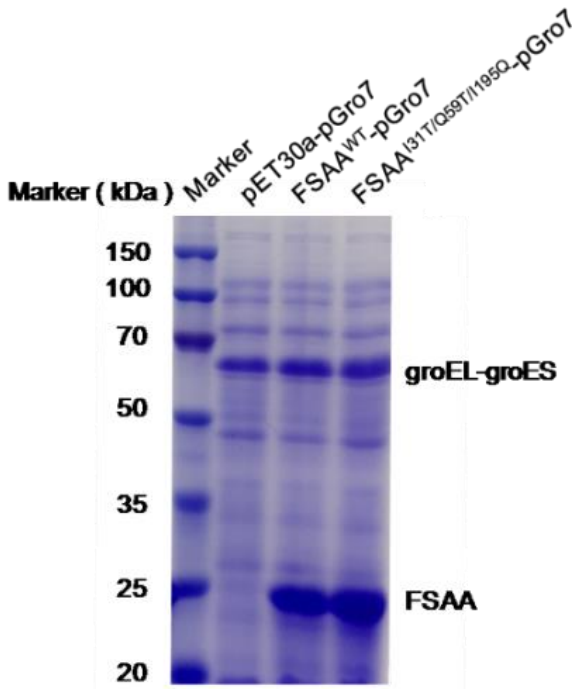

Fig. S7 SDS-PAGE analysis of the cell-free extracts of the whole-cell catalysts.

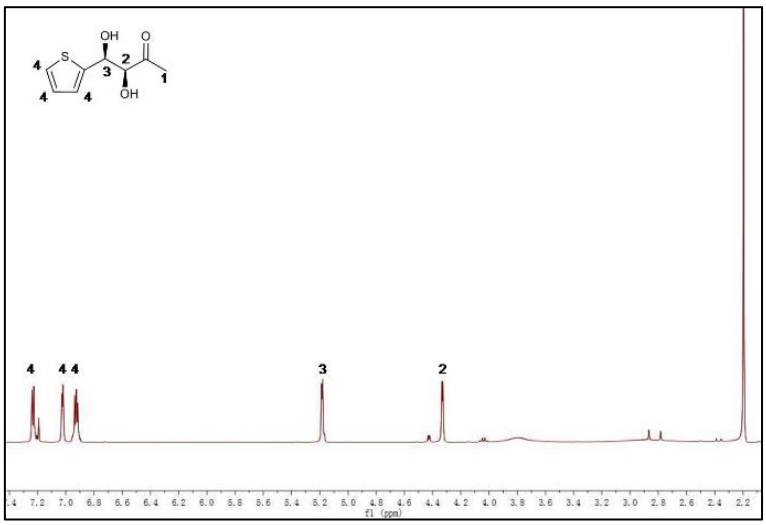

a) (3*S*, 4*S*)-**3a**: ^{1}HNMR (400 MHz, $CDCl_3$), $[\alpha]_D^{22}$ = +24.7 (*c* = 1 in $CHCl_3$) (Units for $[\alpha]$ and *c* are deg $cm^3 g^{-1} dm^{-1}$ and g cm^{-3}, respectively).

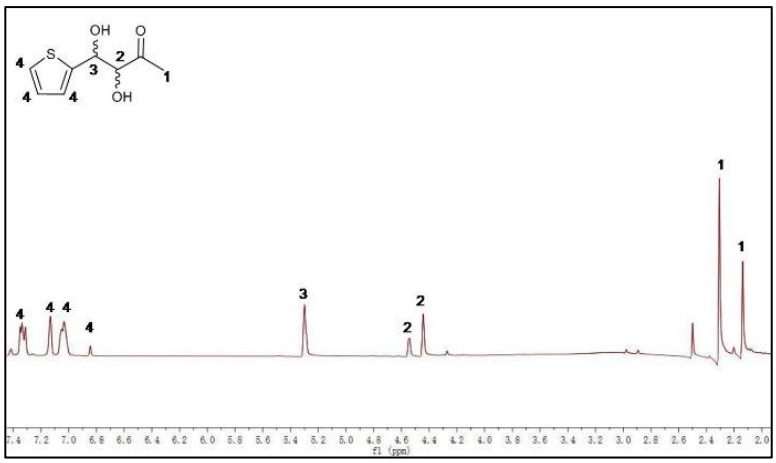

b) Racemic **3a**: ^{1}HNMR (400 MHz, $CDCl_3$).

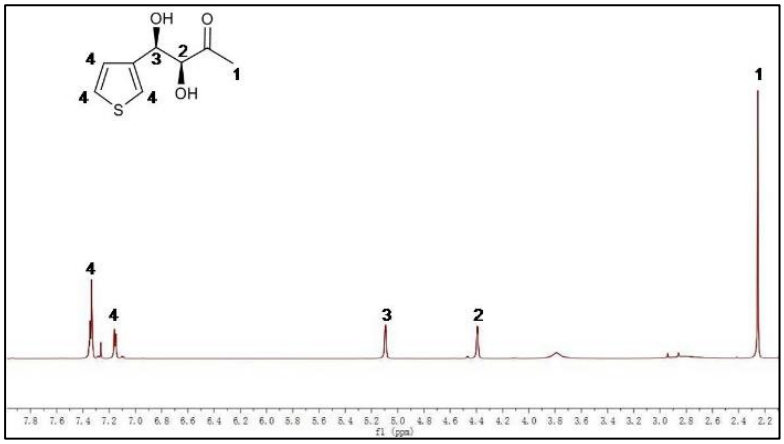

c) **3b** synthesized by I31T/Q59T/I195Q FSAA: ^{1}HNMR (400 MHz, $CDCl_3$), $[\alpha]_D^{22}$ = +19.7 (*c* = 1.37 in $CHCl_3$).

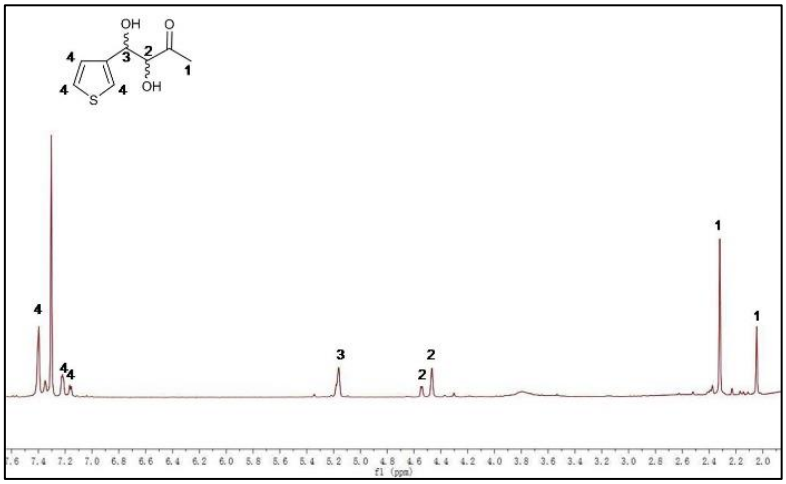

d) Racemic **3b**: ^{1}HNMR (400 MHz, $CDCl_3$).

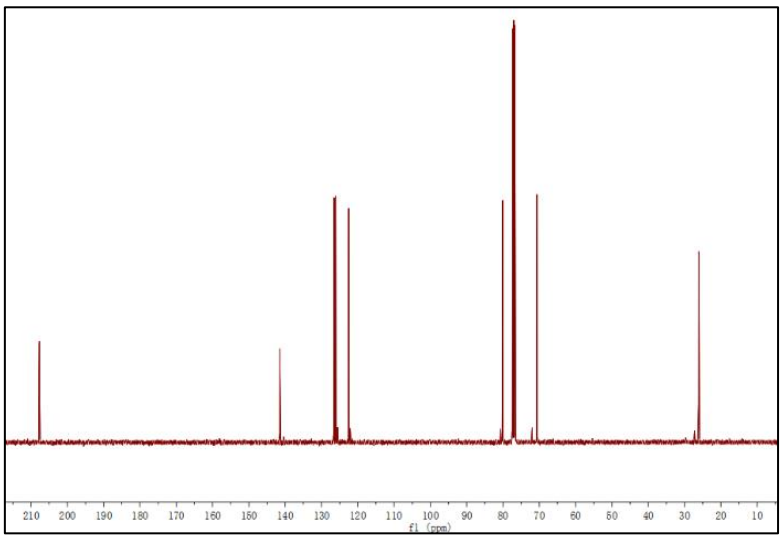

e) **3b** synthesized by I31T/Q59T/I195Q FSAA: ^{13}C NMR (400 MHz, $CDCl_3$): δ 207.67, 141.5, 126.5, 126.1, 80.1, 70.6, 26.1

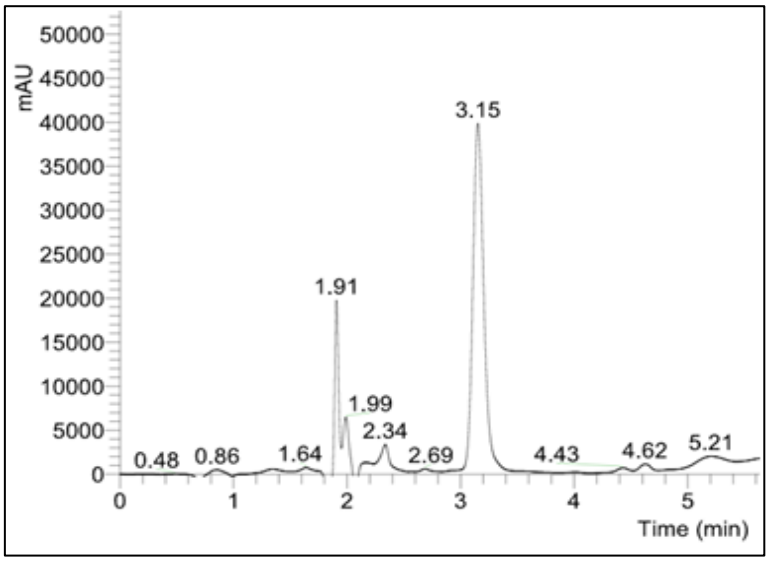

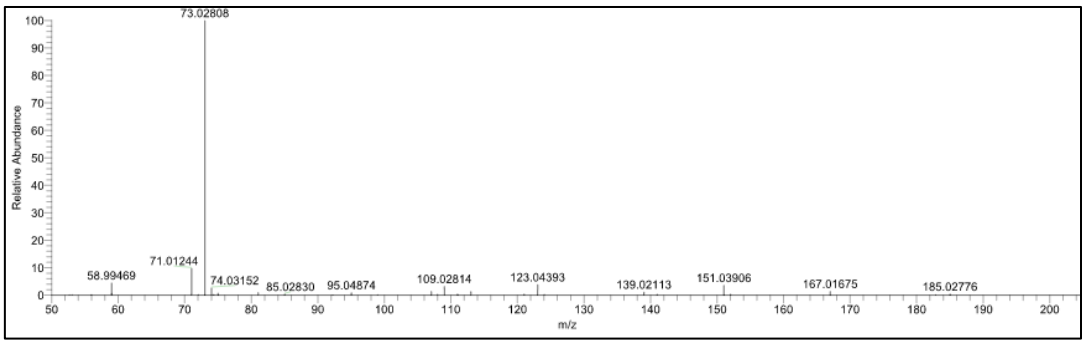

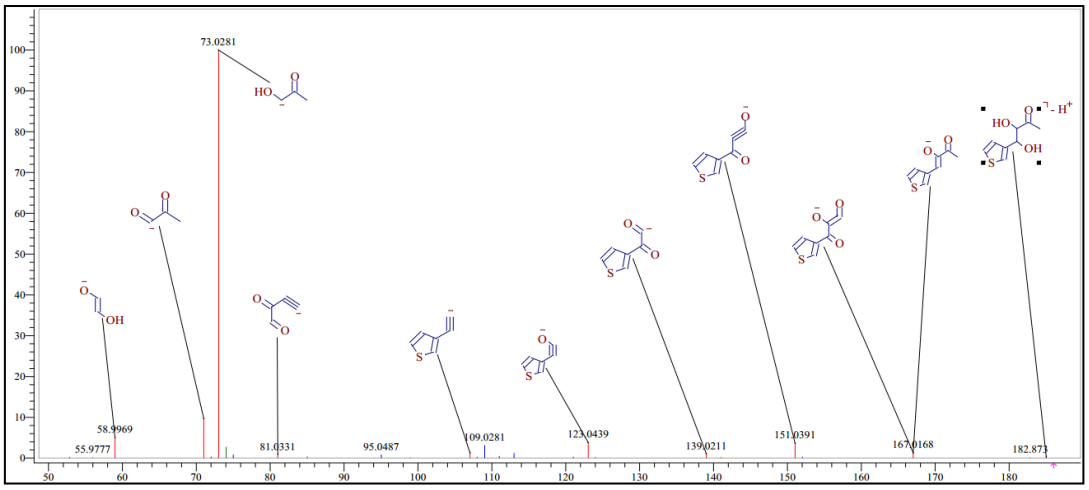

f) HPLC-MS/MS spectrometry of **3b** synthesized by I31T/Q59T/I195Q FSAA. Retention time of **3b**: 3.15 min

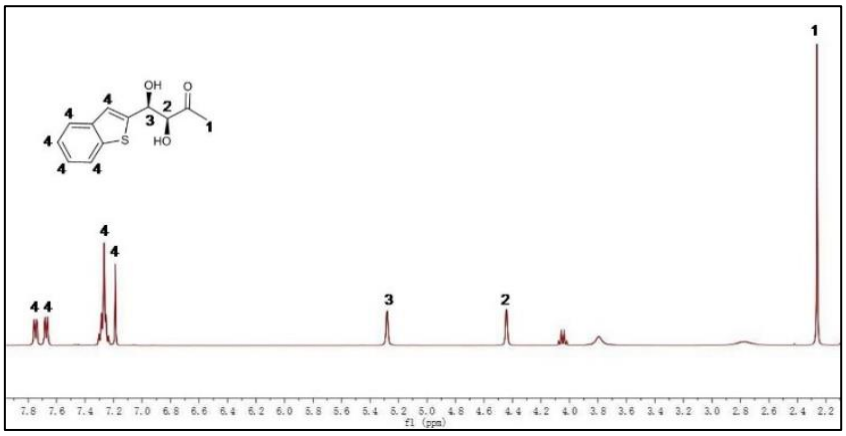

g) (3*S*, 4*S*)-**3c**: ^{1}H NMR (400 MHz, $CDCl_3$), $[\alpha]_D^{23}$ = +9.6 (*c* = 0.523 in $CHCl_3$).

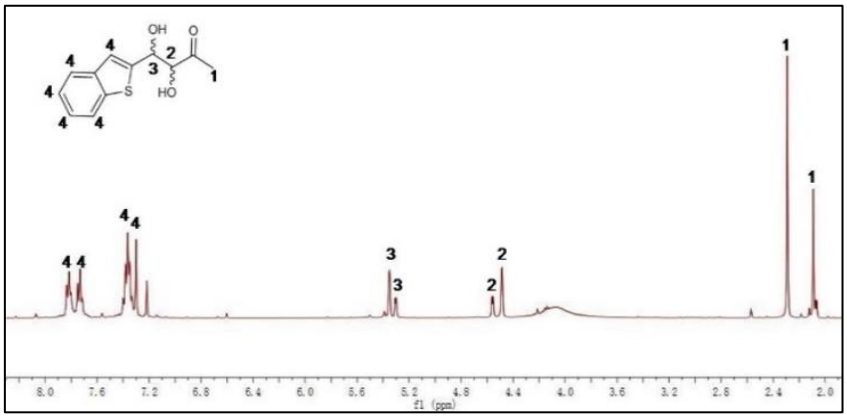

h) Racemic **3c**: ^{1}H NMR (400 MHz, $CDCl_3$).

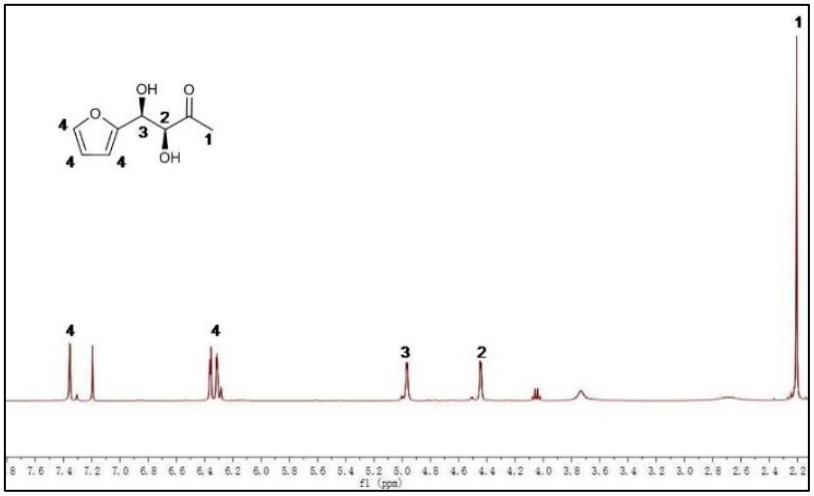

i) **3d** synthesized by I31T/Q59T/I195Q FSAA: 1H NMR (400 MHz, CDCl3), $[\alpha]_D^{23}$ = +11.8(c = 0.83 in CHCl3).

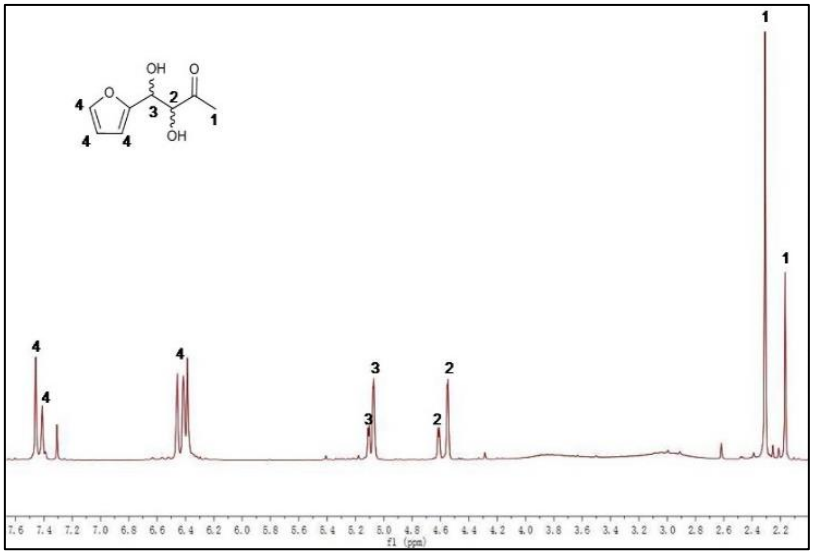

j) Racemic **3d**: ^{1}H NMR (400 MHz, $CDCl_3$).

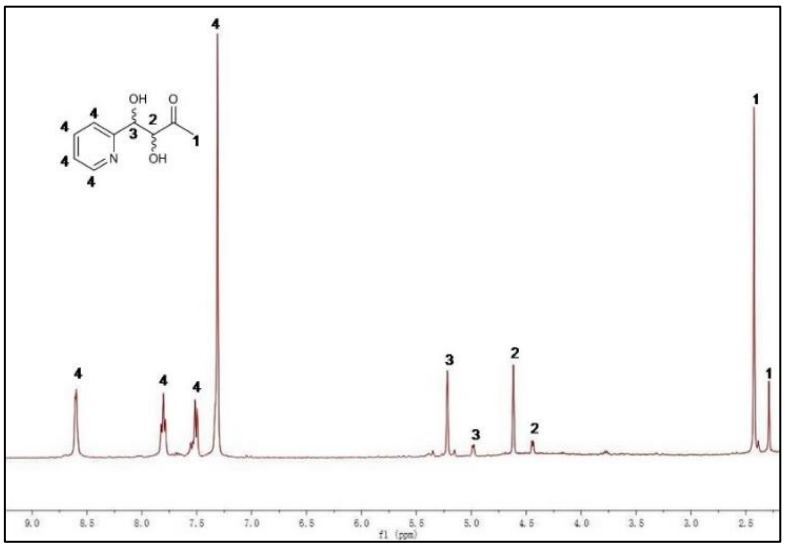

k) Racemic **3e**: ^{1}H NMR (400 MHz, $CDCl_3$).

Fig. S8 NMR and HPLC-MS/MS spectra of products 3**a**-3**e**.

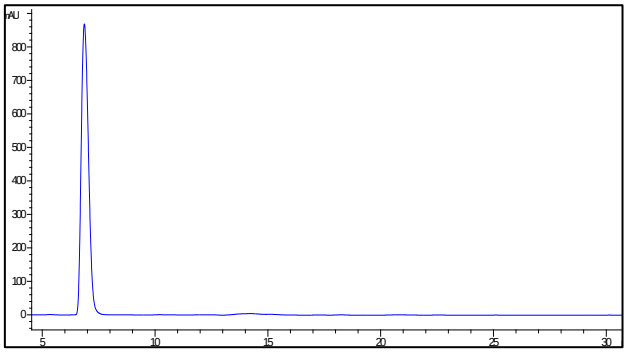

a) Substrate **1a**, retention time: 7 min.

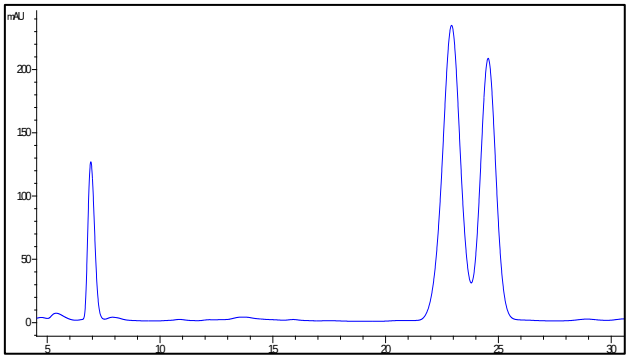

b) Substrate **1a** with racemic **3a** synthesized by NaOH, retention time of racemic **3a**: 23 min and 24.6 min.

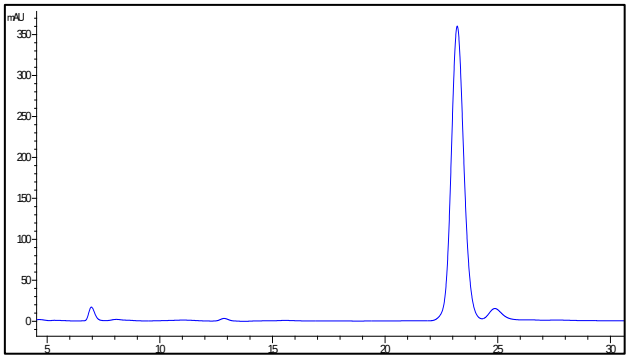

c) **3a** synthesized by wild-type FSAA, retention time: 23 min.

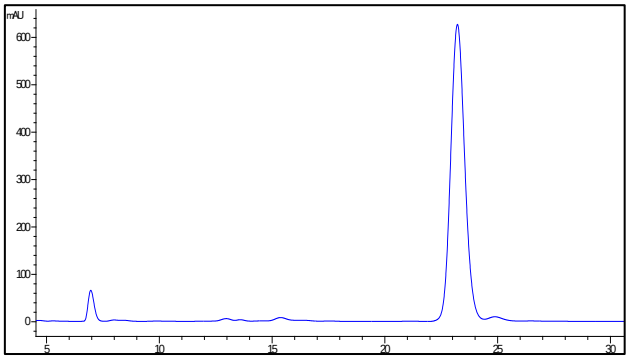

d) **3a** synthesized by I31T/Q59T/I195Q FSAA, retention time: 23 min.

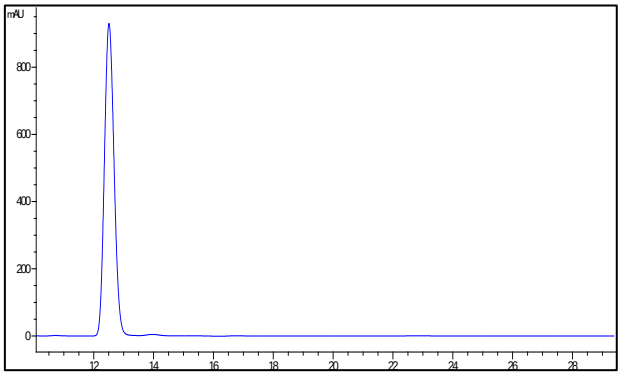

e) Substrate **1b**, retention time: 12.5 min.

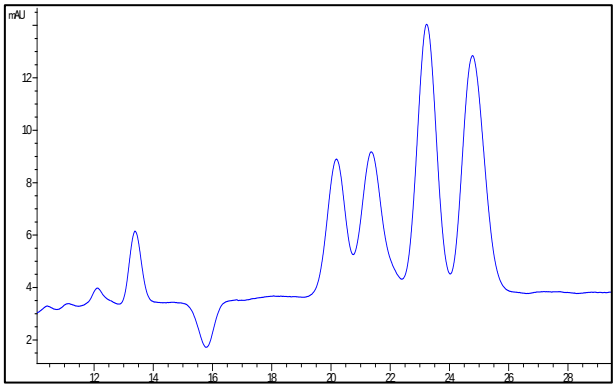

f) Substrate **1b** with racemic **3b** synthesized by NaOH, retention time of racemic **3b**: 20.3 min, 21.5 min 23.3 min and 25.3 min.

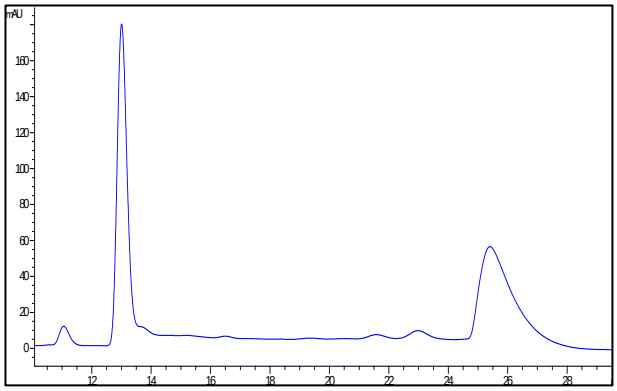

g) **3b** synthesized by wild-type FSAA, retention time: 25.4 min.

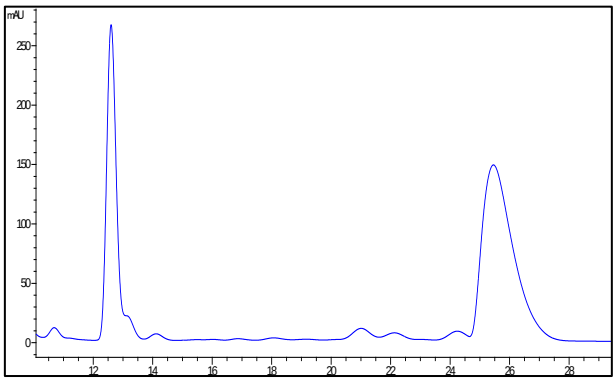

h) **3b** synthesized by I31T/Q59T/I195Q FSAA, retention time: 25.4 min.

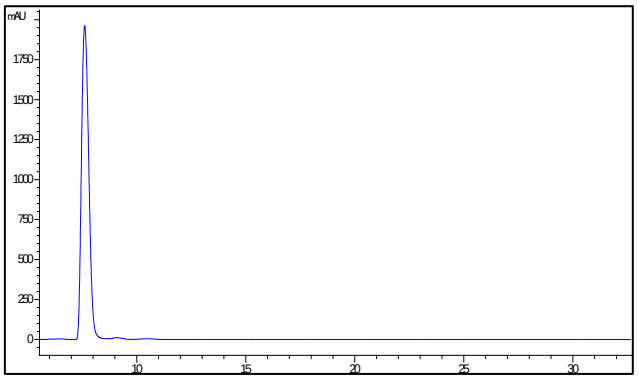

i) Substrate **1c**, retention time: 7.8 min.

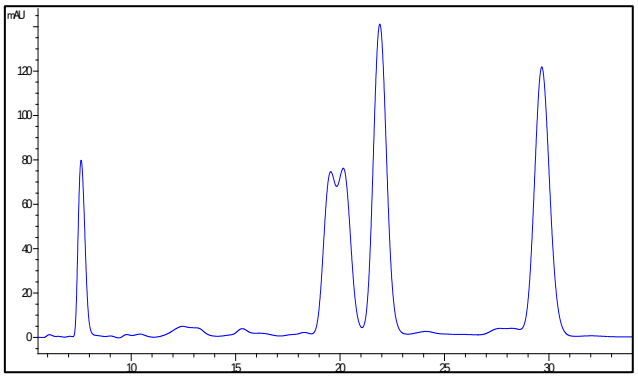

j) Substrate **1c** with racemic **3c** synthesized by NaOH, retention time of racemic **3c**: 19.5 min, 20.3 min, 21.9 min and 29.8 min.

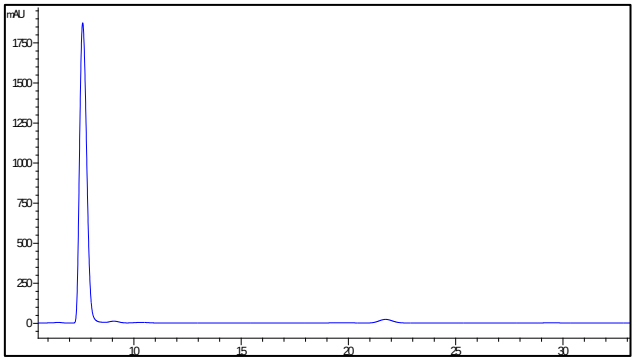

k) **3c** synthesized by wild-type FSAA, retention time: 21.9 min.

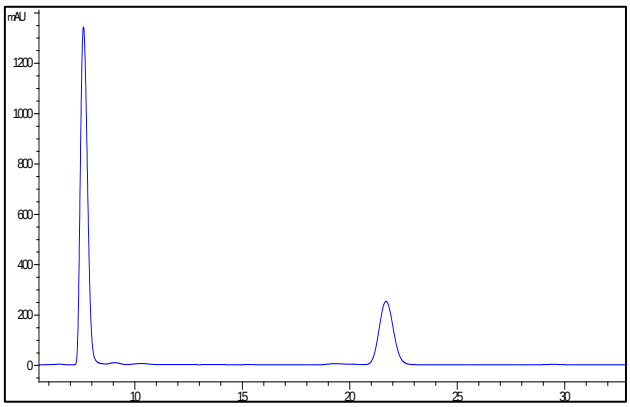

l) **3c** synthesized by I31T/Q59T/I195Q FSAA, retention time: 21.9 min.

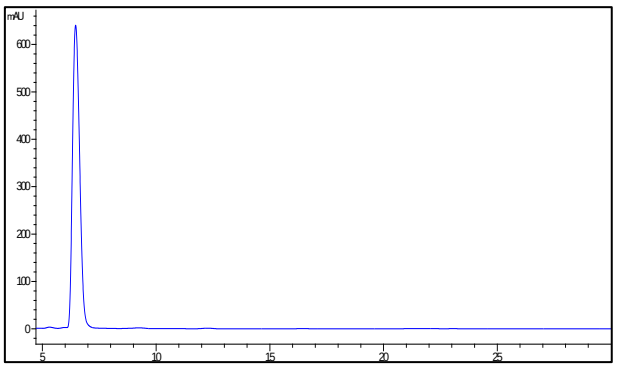

m) Substrate **1d**, retention time: 6.5 min.

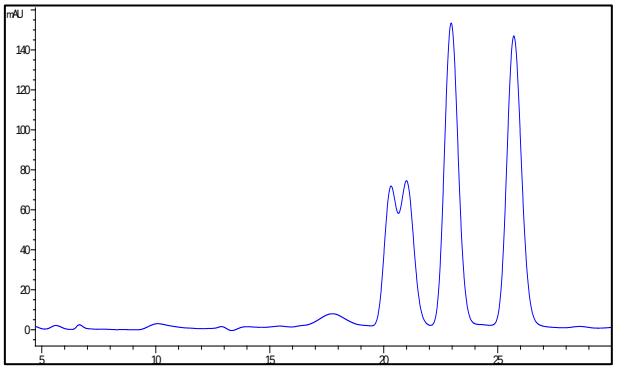

n) Substrate **1d** with racemic **3d** synthesized by NaOH, retention time of racemic **3d**: 20.4 min, 21.3 min, 23 min and 25.8 min.

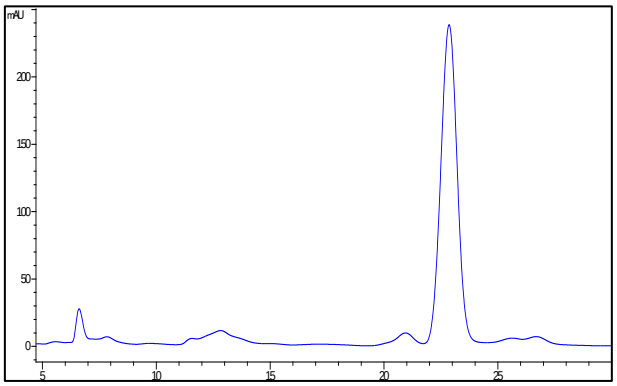

o) **3d** synthesized by wild-type FSAA, retention time: 23 min.

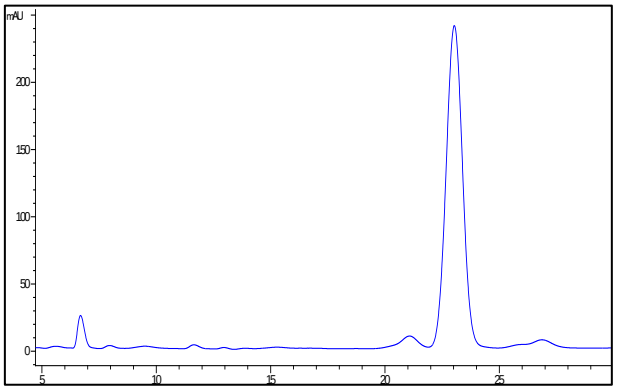

p) **3d** synthesized by I31T/Q59T/I195Q FSAA, retention time: 23 min.

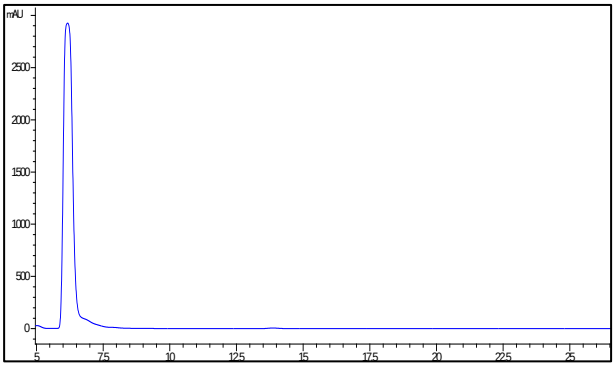

r) Substrate **1e**, retention time: 6.3 min.

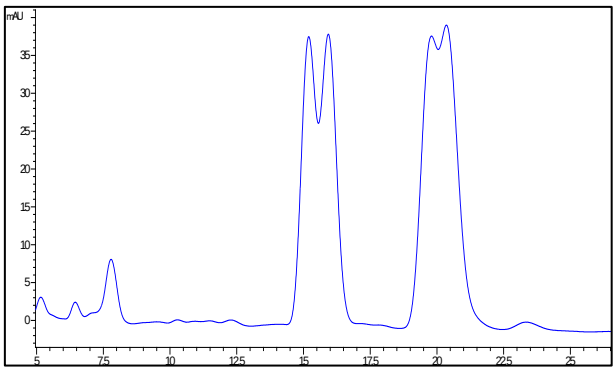

s) Substrate 1e with racemic 3e synthesized by NaOH, retention time of racemic 3e: 15.3 min, 16.2 min, 19.6 min and 20.7 min.

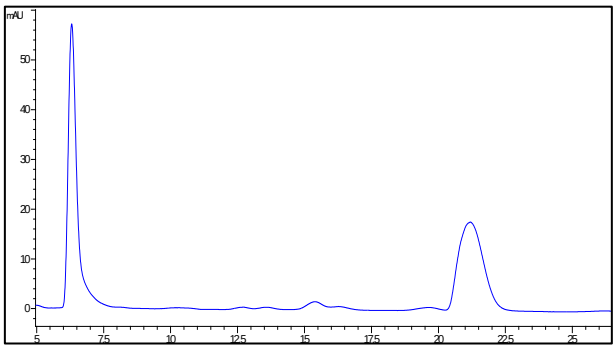

t) **3e** synthesized by wild-type FSAA, retention time: 20.9 min.

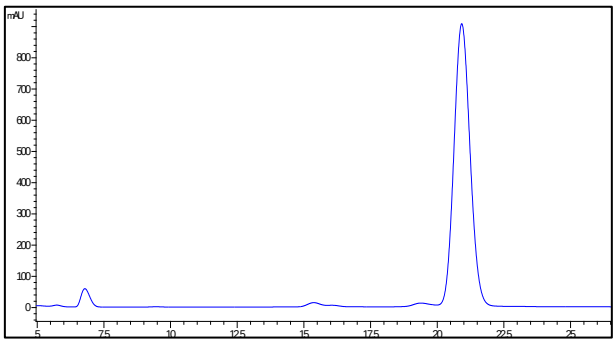

u) **3e** synthesized by I31T/Q59T/I195Q FSAA, retention time: 20.7 min.

Fig. S9 Chiral HPLC analysis of the products synthesized by NaOH, the wild-type FSAA and mutant I31T/Q59T/I195Q FSAA.

References

1. M.-J. Kwon, S.-L. Park, B.-W. Kim, S.-K. Kim and S.-W. Nam, *J. Life Sci.* , 2002, **12** 688-693.
2. L. Stellmacher, T. Sandalova, S. Leptihn, G. Schneider, G. A. Sprenger and A. K. Samland, *ChemCatChem* 2015, **7**, 3140 – 3151.
3. X. Yang, L. Ye, A. Li, C. Yang, H. Yu, J. Gu, F. Guo, L. Jiang, F. Wang and H. Yu, *Catal. Sci. Technol.*, 2017, **7**, 382-386.
4. W. Minor, M. Cymborowski, Z. Otwinowski and M. Chruszcz, *Acta Crystallogr., Sect. D: Biol. Crystallogr.*, 2006, **62**, 859-866.
5. A. J. McCoy, R. W. G. Kunstleve, P. D. Adams, M. D. Winn, L. C. Storoni and R. J. Read, *J. Appl. Crystallogr.*, 2007, **40**, 658-674.
6. P. D. Adams, P. V. Afonine, G. Bunkóczi, V. B. Chen, I. W. Davis, N. Echols, J. J. Headd, L.-W. Hung, G. J. Kapral, R. W. Grosse-Kunstleve, A. J. McCoy, N. W. Moriarty, R. Oeffner, R. J. Read, D. C. Richardson, J. S. Richardson, T. C. Terwilliger and P. H. Zwart, *Acta Crystallogr., Sect. D: Biol. Crystallogr.*, 2010, **66**, 213-221.
7. P. Emsley, B. Lohkamp, W. G. Scott and K. Cowtan, *Acta Crystallogr., Sect. D: Biol. Crystallogr.*, 2010, **66**, 486-501.
8. S. Thorell, M. Schürmann, G. A. Sprenger and G. Schneider, *J. Mol. Biol.*, 2002, **319**, 161-171.
9. M. Gutierrez, T. Parella, J. Joglar, J. Bujons and P. Clapés, *Chem. Commun.*, 2011, **47**, 5762-5764.
10. A. Szekrenyi, A. Soler, X. Garrabou, C. Guerard-Helaine, T. Parella, J. Joglar, M. Lemaire, J. Bujons and P. Clapés, *Chem. Eur. J.*, 2014, **20**, 12572-12583.
11. D.A. Case, V. Babin, J.T. Berryman, R.M. Betz, Q. Cai, D.S. Cerutti, T.E. Cheatham, III, T.A. Darden, R.E. Duke, H. Gohlke, A.W. Goetz, S. Gusarov, N. Homeyer, P. Janowski, J. Kaus, I. Kolossváry, A. Kovalenko, T.S. Lee, S. LeGrand, T. Luchko, R. Luo, B. Madej, K.M. Merz, F. Paesani, D.R. Roe, A. Roitberg, C. Sagui, R. Salomon-Ferrer, G. Seabra, C.L. Simmerling, W. Smith, J. Swails, R.C. Walker, J. Wang, R.M. Wolf, X. Wu and P.A. Kollman (2014), AMBER 14, University of California, San Francisco.
12. W. Humphrey, A. Dalke and K. Schulten, *J. Molec. Graphics*, 1996, **14**, 33-38.
13. J. D. Durrant, L. Votapka, J. Sorensen and R. E. Amaro, *J. Chem. Theory Comput.*, 2014, **10**, 5047-5056.
14. E. F. Pettersen, T. D. Goddard, C. C. Huang, G. S. Couch, D. M. Greenblatt, E. C. Meng and T. E. Ferrin, *J. Comput. Chem.*, 2004, **25**, 1605-1612.
15. S. Yuan, H. C. S. Chan, S. Filipek and H. Vogel, *Structure*, 2016, **24**, 2041-2042.
16. F. Secci, E. Cadoni, C. Fattuoni, A. Frongia, G. Bruno and F. Nicolò, *Tetrahedron*, 2012, **68**, 4773-4781.